JACS
JOURNAL OF THE AMERICAN CHEMICAL SOCIETY
Communication
pubs.acs.org/JACS

Direct Growth of High-Quality Graphene on High-κ Dielectric $SrTiO_3$ Substrates

Jingyu Sun,[†] Teng Gao,[†] Xiuju Song,[†] Yanfei Zhao,[§] Yuanwei Lin,[†] Huichao Wang,[§] Donglin Ma,[†] Yubin Chen,[†] Wenfeng Xiang,[∥] Jian Wang,[§] Yanfeng Zhang,*[,†,‡] and Zhongfan Liu*[,†]

[†]Center for Nanochemistry (CNC), Beijing National Laboratory for Molecular Sciences, College of Chemistry and Molecular Engineering, Peking University, Beijing 100871, P. R. China

[‡]Department of Materials Science and Engineering, College of Engineering, Peking University, Beijing 100871, P. R. China

[§]International Center for Quantum Materials, School of Physics, Peking University, Beijing 100871, P. R. China

[∥]State Key Laboratory of Heavy Oil Processing, China University of Petroleum, Beijing 102249, P. R. China

Supporting Information

ABSTRACT: High-quality monolayer graphene was synthesized on high-κ dielectric single crystal $SrTiO_3$ (STO) substrates by a facile metal-catalyst-free chemical vapor deposition process. The as-grown graphene sample was suitable for fabricating a high performance field-effect transistor (FET), followed by a far lower operation voltage compared to that of a SiO_2-gated FET and carrier motilities of approximately 870−1050 $cm^2 \cdot V^{-1} \cdot s^{-1}$ in air at rt. The directly grown high-quality graphene on STO makes it a perfect candidate for designing transfer-free, energy-saving, and batch production of FET arrays.

Graphene is deemed as one of the most attractive candidate materials for next-generation electrical and optical devices due to its unique properties.[1−4] In order to fulfill the potential of graphene in real technological applications, various methods targeting its rational synthesis have been pursued, mainly including mechanical and chemical exfoliation,[1] SiC thermal decomposition,[5] and chemical vapor deposition (CVD).[6] In particular, CVD approaches employing Cu,[6] Ni,[7] and other metals (such as Pt[8]) as catalysts have been proven promising with regards to the synthesis of high-quality, large domain size, and uniform graphene. However, the inevitable transfer process from metal onto dielectric substrates is nevertheless tedious and cost-ineffective, which might also introduce wrinkles, breakages, defects, and metallic contaminations/residues on the graphene samples. To this end, direct fabrications of graphene on insulating substrates such as MgO,[9] SiO_2,[10−13] Al_2O_3,[14−16] and Si_3N_4[17,18] by metal-catalyst-free CVD have been demonstrated, offering great opportunities for directly fabricating graphene devices without any transfer process. The synthesis processes involved always required ultrahigh growth temperatures normally above 1400 °C,[14,16] an inconvenient apparatus setup using plasma-enhanced CVD,[11,19] and/or extremely long growth times even up to 4320 min.[18] Moreover, typical graphene products could suffer from lower crystal quality, inferior thickness uniformity, and/or degraded properties (as compared with growth on metals). From a technological point of view, the selection of more suitable insulating substrates for direct graphene growth is of great importance since the substrates, serving as gate insulators in electronics (e.g., field effect transistor (FET)), have a strong influence on the properties of graphene and hence the performances of devices.[20]

In this regard, the usage of high-κ dielectric substrates rather than low-κ SiO_2 ($\kappa \approx 4$) would be promising in providing reduced gate leakage, improved gate capacitance, and better gate modulation.[21] Moreover, carrier scattering issues caused by surface roughness and charge fluctuations on SiO_2 substrates could hinder further integration of SiO_2-gated graphene FETs.[21−23] Therefore, direct growth of graphene on high-κ, scatter-screening dielectric substrates becomes greatly desirable. Herein we demonstrate that, on $SrTiO_3$ (STO), a transparent, high-κ perovskite insulator bearing superior thermal stabilities and versatile application potentials,[24−26] facile metal-catalyst-free CVD growth of high-quality graphene was realized, offering a deeper understanding of direct growth of graphene on insulating substrates. The resulted graphene sample included a highly uniform monolayer and large area (with the size only limited by the crystal size of STO). With the unique directly grown graphene/STO sample, we have observed for the first time bipolar FET behavior on the STO-gated FET, along with a low operation voltage. The intriguing magneto-transport properties of as-grown graphene/STO samples have also been investigated.

The direct growth of graphene on STO (001) substrates was carried out by a simple atmospheric CH_4-CVD process without the aid of any metallic species (see Supporting Information (SI)), where elemental characterizations by X-ray diffraction and full X-ray photoelectron spectroscopy (XPS) measurements of as-grown samples were performed to ensure a complete metal-free process had taken place (Figure S1). Figure 1a illustrates that the growth of graphene on STO is governed by an in-plane propagation process of carbon species. This is reflected by the atomic force microscopy (AFM) examinations of the growth evolution, as characterized by graphene nanoislands, continuous film with irregular voids, and complete layers decorated with graphene wrinkles when experiencing 60, 120, and 180 min CVD ($Ar/H_2/CH_4$: 100/

Received: March 11, 2014
Published: April 18, 2014

   dx.doi.org/10.1021/ja5022602 | J. Am. Chem. Soc. 2014, 136, 6574−6577

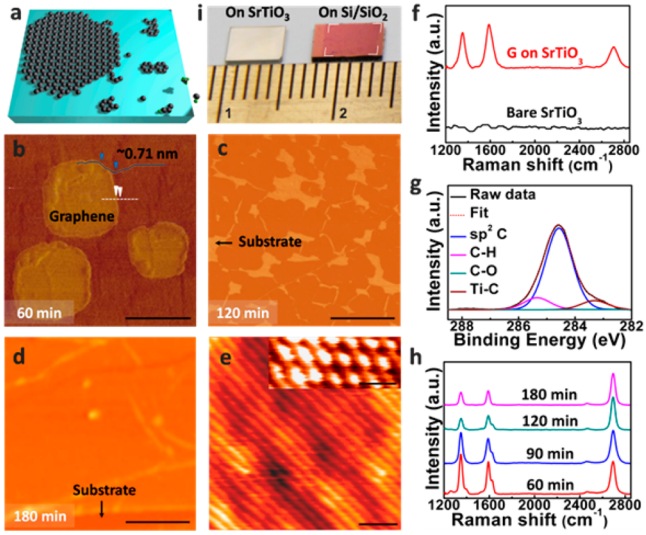

Figure 1. Investigation of growth evolution and characterization of as-grown graphene on STO (001). (a) Schematic of graphene growth on STO substrates. (b–d) Morphology evolutions of as-grown samples experiencing various CVD growth time as characterized by AFM images and the section view (as an insert). Scale bars: (b) 250 nm. (c, d) 1 μm. (e) STM image (V_s = 0.7 μV, I_t = 18 nA) of a graphene film. Scale bar: 1 nm. Inset: Atomic resolved STM image of graphene honeycomb lattice. Scale bar: 0.5 nm. (f) Representative Raman spectra (514 nm laser wavelength) of as-grown graphene and bare STO substrates. (g) C 1s XPS spectrum of as-grown graphene. (h) Time-dependent growth of graphene (after transferred onto Si/SiO_2 substrate for a better inspection) investigated by Raman spectroscopy. All the Raman spectra are normalized to 2D peak intensity. (i) Photograph of an as-grown graphene film on STO and a transferred graphene film to Si/SiO_2 (300 nm thickness) substrate.

50/2.5 sccm) (Figure 1b–d; also shown in Figure S2), respectively. Note that the nanoislands, possessing a similar height of ~0.71 nm (typical for graphene on SiO_2),[7] expand their sizes and merge with each other to form a complete film, guaranteeing the uniform layer thickness. This growth feature is consistent with the growth trends reported in previous studies using SiO_2[10] and Al_2O_3[15] as substrates.

The formation of graphene on STO was further probed with atomic-scale characterizations by scanning tunneling microscopy (STM) (Figure 1e and inset, and Figure S3), clearly revealing the graphene lattices with a lattice constant of ~0.246 nm.[19] Moreover, a typical Raman spectrum of as-grown graphene on STO (Figure 1f) displays three characteristic peaks of graphene at the D band (1350 cm^{-1}), G band (1597 cm^{-1}), and 2D band (2695 cm^{-1}), which are totally absent from the spectrum of the bare STO substrate (black curve), providing more spectroscopic proof of the graphene formation. However, it has been found that the 2D peak of directly grown graphene on the STO substrate (red curve) cannot be unambiguously revealed due to the possible substrate screening effect (strain induced by the lattice mismatch and/or strong interaction caused by chemical bonding between the graphene and substrate, etc.), the case of which is similar to that regarding graphene grown on SiC.[27] This interaction was partially reflected by the C 1s XPS measurement (Figure 1g), with the presence of the Ti–C peak (283.4 eV), in addition to the featured signals of graphene with an sp^2 carbon peak (284.8 eV) and C–H peak (285.3 eV). Corresponding time-dependent growth evolution of graphene (shown in Figure 1b–d) was further investigated by Raman spectroscopy (Figure 1h), revealing that the 180 min CVD process enabled the formation of high-quality monolayer graphene. Notably, the area of the complete monolayer can only be limited by the size of the STO substrate, as evidenced by a photograph of the as-grown and as-transferred samples on Si/SiO_2 (Figure 1i) showing a uniform contrast. Moreover, graphene covered STO samples exhibit special optical performances (Figure S4), the study of which is still ongoing.

The high thickness uniformity and the monolayer nature (>95%) of our prepared graphene was confirmed by characterizing the transferred samples to Si/SiO_2 substrates. The graphene film (growth time 180 min) appears in uniform contrast when inspected by optical microscopy (OM) and SEM (Figure 2a, b), reaching full substrate coverage except for the

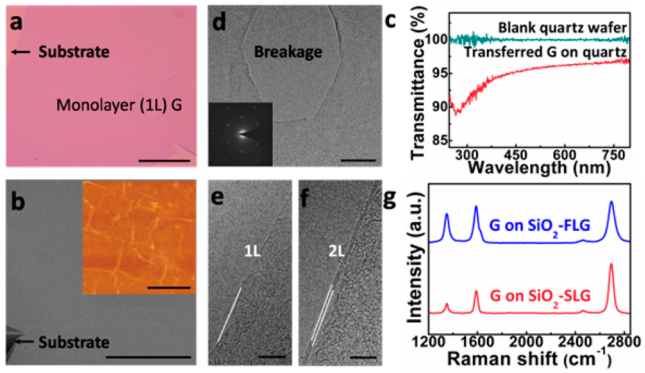

Figure 2. Analysis of large-area uniform monolayer graphene produced by metal-catalyst-free CVD on STO (001) substrates. (a) OM image of a graphene film transferred to Si/SiO_2. Scale bar: 20 μm. (b) SEM image of the transferred graphene film. Scale bar: 50 μm. Inset: corresponding AFM image. Scale bar: 1 μm. (c) Transmittance spectra of transferred graphene on quartz. (d) Low-magnification TEM image of the graphene film. Scale bar: 100 nm. Inset: SAED pattern displaying one set of hexagonal pattern. (e, f) High-resolution TEM images of the universally existed single layer (>95%) and a seldom noticed bilayer graphene (<5%). Scale bars: 5 nm. (g) Representative Raman spectra (514 nm laser wavelength) of as-transferred monolayer graphene.

small breakages due to the transfer process. AFM characterization (inset in Figure 2b) again supports the successful formation of continuous, uniform monolayer graphene, as evidenced by the formation of graphene wrinkles. UV–vis spectroscopy examined at a wavelength of 550 nm exhibits transmittance at 96.4% (Figure 2c), providing more macroscopic evidence of the uniform monolayer nature of the graphene films, probably facilitating its applications in transparent electrodes, optoelectronic devices, and so on.

A transmission electron microscopy (TEM) investigation was conducted to probe the detailed microstructure and layer information on the fabricated graphene. It is worth mentioning that we have employed an advantageous two-stage transfer approach to guarantee a far cleaner preparation of the TEM samples (Figures S5 and S6) compared to others. Figure 2d displays a low-magnification TEM view of the rather clean graphene films (growth time 180 min), where the edges of the sheet breakage allow us to directly identify the layer numbers. The selected-area electron diffraction (SAED) pattern (inset in Figure 2d) manifests one set of a hexagonal symmetrical pattern, justifying the high crystallinity of graphene films.

dx.doi.org/10.1021/ja5022602 | J. Am. Chem. Soc. 2014, 136, 6574–6577

Moreover, the high-resolution TEM image on the film edge (Figure 2e) indicates that the film is predominantly single layer graphene (>95%), with bilayer graphene occasionally detected (Figure 2f).

Full and C 1s XPS spectra of the as-transferred graphene on SiO_2 are shown in Figure S7. As previously mentioned, the as-grown graphene was then transferred to Si/SiO_2 substrates to facilitate a characteristic property evaluation by Raman spectroscopy. The pink curve of transferred graphene in Figure 2g reveals a sharp 2D peak located at ~2692 cm^{-1} with a high I_{2D}/I_G ratio (>2) and a full width at half-maximum (fwhm) of 37 cm^{-1}, verifying the formation of single layer graphene (SLG). In contrast, a representative Raman spectrum of few-layer graphene (FLG) was also recorded (mainly from the edged areas of samples), which is featured by a lower I_{2D}/I_G ratio (<1.5) and a broader fwhm of 60 cm^{-1} (blue curve). Moreover, the discernible down-shifted Raman bands of transferred graphene are observed to suggest a strain effect between graphene and STO substrates, which might be generated from the relaxation of compressive stress induced by the distinct thermal expansion coefficient between graphene (-8.0×10^{-6} K^{-1} at 300 K) and STO (9.4×10^{-6} K^{-1} at 300 K), or from a considerable lattice mismatch effect (a_{graphene} = 2.468 Å and $a_{\text{STO (001)}}$ = 3.905 Å). Such a trend is consistent with previously reported results regarding the metal-free synthesis of graphene on Al_2O_3[15] and Si_3N_4.[17] Note that this strain relaxation phenomenon can also be observed when using STO (111) and STO (110) as the growth substrate in our study (Figure S8).

Herein our work implies that high-quality monolayer graphene with uniform thickness can be fabricated on STO substrates within 180 min of growth under a relatively low temperature (comparable with growth on metals), which may address the advanced catalytic ability of STO in terms of catalyzing graphene formation compared to that of other oxides (SiO_2 and Si_3N_4). It is known that the surface oxygen is beneficial to the direct nucleation and growth of graphene on insulating substrates; in our case, we speculate that the presence of surface titanium and oxygen on the STO (001) substrate could exert a synergistic effect on the graphene synthesis (Figure 1g). In turn, the growth of graphene on STO substrates can be realized under a broad parameter window, where temperature-dependent studies by Raman spectroscopy were performed to investigate the growth dynamics (Figure S9). The as-grown homogeneous graphene can be readily transferred to arbitrary substrates to further potential applications (such as transparent conductive films), e.g. to a polyethylene terephthalate (PET) sheet exhibiting high light transparency, as shown in Figure 3a. Specifically, to examine in detail the 2D homogeneity and quality of monolayer graphene grown for 180 min at 1050 °C, point Raman spectra were randomly collected from 130 points over a 3 × 3 mm^2 area, leading to the presentation of six randomly collected spectra (Figure 3b), as well as the plot of a histogram of the I_{2D}/I_G ratio (Figure 3c), and a histogram of the $fwhm_{2D}$ distribution (Figure 3d). Furthermore, Raman mapping of I_G and I_{2D} over the marked area in the OM image (Figure 3e) is shown in Figure 3f and g with rather uniform color contrasts, respectively, further ascertaining the uniformity of produced graphene films in macroscopic scales.

The sheet resistances of graphene films grown directly on STO substrates have been probed, with the obtained lowest value reaching 950 Ω·sq^{-1} (growth time: 300 min). A

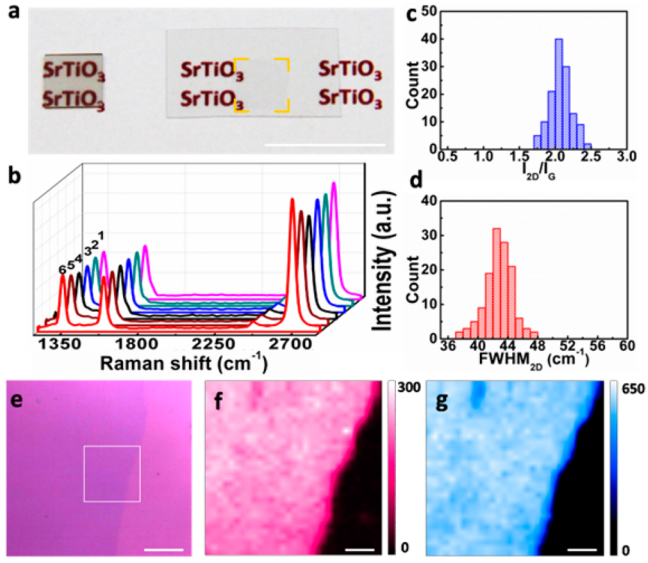

Figure 3. Investigations of the thickness uniformity of synthesized graphene films by Raman spectroscopy. (a) Photograph of an as-grown graphene/STO sample (left) and a transferred graphene film to a PET sheet (right), showing its uniformity and good visible light transparency. Scale bar: 1 cm. (b–d) Plot of (b) six typically collected spectra, and histograms of the (c) I_{2D}/I_G ratios and (d) $fwhm_{2D}$ distribution over a 3 × 3 mm^2 sample area. (e) OM image of a graphene film with a mark indicating the mapping region. Scale bar: 20 μm. (f, g) Raman mapping of the marked region in (e). (f) G peak. (g) 2D peak. Scale bars: 5 μm.

comparison between the sheet resistances of the graphene prepared in this work and those of reported graphene is depicted in Figure 4a as a function of growth time, revealing

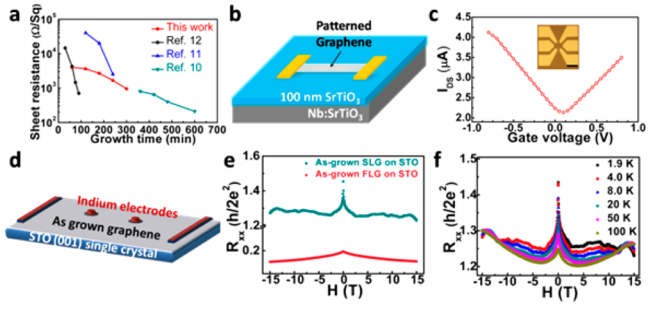

Figure 4. Electrical and magneto-transport properties of graphene directly grown on STO substrates. (a) Comparison of the sheet resistances of graphene obtained in this work and others in the literature. (b) Schematic top-view of graphene FET fabricated on an STO/Nb-doped STO substrate. (c) Transfer curve of the FET device at V_{DS} = 0.01 V in air. Inset: OM image of an individual device. Scale bar: 50 μm. (d) Schematic construction of graphene/STO based device for magneto-transport measurements. (e, f) MR behaviors of as-grown samples as a function of magnetic field.

that the quality of our graphene is comparable to those of others. To further examine the electrical properties of as-grown graphene, back-gated graphene FET was fabricated on an STO (100 nm thick)/Nb-doped STO substrate using a standard photolithography technique (Figure 4b and SI). Surprisingly, the transfer curve (drain current I_{DS} vs gate voltage V_G) in Figure 4c shows that bipolar FET characteristics of the device can be achieved with a very small bias operation of the back gate (~0.11 V), owing to the large dielectric constant of the

dx.doi.org/10.1021/ja5022602 | J. Am. Chem. Soc. 2014, 136, 6574–6577

insulating STO layer. This observation is consistent with that reported in a previous study, where mechanically exfoliated graphene transferred on an STO/Nb-doped STO substrate was used.[21] The carrier mobilities estimated from the transfer curves range from about 870 to 1050 $cm^2 \cdot V^{-1} \cdot s^{-1}$. Figure 4e shows the magneto-resistance (MR) behaviors of as-grown SLG and FLG on STO (the device construction illustrated in Figure 4d and measurements conducted at 1.9 K), where a weak localization effect can be observed near zero magnetic field. Under a higher perpendicular field, the MR of SLG shows apparent oscillations while being absent from those of FLG and FLG grown on SiO_2 under identical conditions (Figure S10). Furthermore, investigations on the MR of the SLG sample as a function of the magnetic field at different temperatures were performed. As shown in Figure 4f, the MR fluctuations are almost reproducible at distinct temperatures ranging from 1.9 to 100 K with decreasing amplitudes, which is likely an indication of universal conductance fluctuations.[28]

In summary, large-area, highly uniform monolayer graphene was synthesized for the first time on single crystal STO substrates by a facile CVD process. The as-grown graphene on STO exhibits unique electronic and optical properties and hence shows promise for applications in transfer-free electronic devices for energy-saving, high-performance FET and transparent electrodes.

■ ASSOCIATED CONTENT

Supporting Information

Experimental protocols and additional description, characterization, and data analysis. This material is available free of charge via the Internet at http://pubs.acs.org.

■ AUTHOR INFORMATION

Corresponding Authors

zfliu@pku.edu.cn
yanfengzhang@pku.edu.cn

Notes

The authors declare no competing financial interest.

■ ACKNOWLEDGMENTS

This work was financially supported by the Ministry of Science and Technology of China (Grants 2013CB932603, 2012CB933404, 2011CB933003, 2011CB921903, 2013CB934600), the National Natural Science Foundation of China (Grants 51290272, 51121091, 51222201, 11222434), and the Ministry of Education (20120001130010).

■ REFERENCES

(1) Novoselov, K. S.; Geim, A. K.; Morozov, S. V.; Jiang, D.; Zhang, Y.; Dubonos, S. V.; Grigorieva, I. V.; Firsov, A. A. *Science* **2004**, *306*, 666.

(2) Yan, K.; Fu, L.; Peng, H. L.; Liu, Z. F. *Acc. Chem. Res.* **2013**, *46*, 2263.

(3) Wu, D.; Yan, K.; Zhou, Y.; Wang, H.; Lin, L.; Peng, H. L.; Liu, Z. F. *J. Am. Chem. Soc.* **2013**, *135*, 10926.

(4) Zhang, C.; Fu, L.; Zhang, Y. F.; Liu, Z. F. *Acta Chim. Sinica* **2013**, *71*, 308.

(5) Berger, C.; Song, Z. M.; Li, X. B.; Wu, X. S.; Brown, N.; Naud, C.; Mayou, D.; Li, T. B.; Hass, J.; Marchenkov, A. N.; Conrad, E. H.; First, P. N.; de Heer, W. A. *Science* **2006**, *312*, 1191.

(6) Li, X.; Cai, W.; An, J.; Kim, S.; Nah, J.; Yang, D.; Piner, R.; Velamakanni, A.; Jung, I.; Tutuc, E.; Banerjee, S. K.; Colombo, L.; Ruoff, R. S. *Science* **2009**, *324*, 1312.

(7) Reina, A.; Jia, X.; Ho, J.; Nezich, D.; Son, H.; Bulovic, V.; Dresselhaus, M. S.; Kong, J. *Nano Lett.* **2009**, *9*, 30.

(8) Gao, L.; Ren, W.; Xu, H.; Jin, L.; Wang, Z.; Ma, T.; Ma, L.-P.; Zhang, Z.; Fu, Q.; Peng, L.-M.; Bao, X.; Cheng, H.-M. *Nat. Commun.* **2012**, *3*, 699.

(9) Ruemmeli, M. H.; Bachmatiuk, A.; Scott, A.; Boerrnert, F.; Warner, J. H.; Hoffman, V.; Lin, J.-H.; Cuniberti, G.; Buechner, B. *ACS Nano* **2010**, *4*, 4206.

(10) Chen, J.; Wen, Y.; Guo, Y.; Wu, B.; Huang, L.; Xue, Y.; Geng, D.; Wang, D.; Yu, G.; Liu, Y. *J. Am. Chem. Soc.* **2011**, *133*, 17548.

(11) Zhang, L.; Shi, Z.; Wang, Y.; Yang, R.; Shi, D.; Zhang, G. *Nano Res.* **2011**, *4*, 315.

(12) Bi, H.; Sun, S.; Huang, F.; Xie, X.; Jiang, M. *J. Mater. Chem.* **2012**, *22*, 411.

(13) Medina, H.; Lin, Y.-C.; Jin, C.; Lu, C.-C.; Yeh, C.-H.; Huang, K.-P.; Suenaga, K.; Robertson, J.; Chiu, P.-W. *Adv. Funct. Mater.* **2012**, *22*, 2123.

(14) Fanton, M. A.; Robinson, J. A.; Puls, C.; Liu, Y.; Hollander, M. J.; Weiland, B. E.; LaBella, M.; Trumbull, K.; Kasarda, R.; Howsare, C.; Stitt, J.; Snyder, D. W. *ACS Nano* **2011**, *5*, 8062.

(15) Song, H. J.; Son, M.; Park, C.; Lim, H.; Levendorf, M. P.; Tsen, A. W.; Park, J.; Choi, H. C. *Nanoscale* **2012**, *4*, 3050.

(16) Hwang, J.; Kim, M.; Campbell, D.; Alsalman, H. A.; Kwak, J. Y.; Shivaraman, S.; Woll, A. R.; Singh, A. K.; Hennig, R. G.; Gorantla, S.; Rummeli, M. H.; Spencer, M. G. *ACS Nano* **2013**, *7*, 385.

(17) Chen, J.; Guo, Y.; Wen, Y.; Huang, L.; Xue, Y.; Geng, D.; Wu, B.; Luo, B.; Yu, G.; Liu, Y. *Adv. Mater.* **2013**, *25*, 992.

(18) Chen, J.; Guo, Y.; Jiang, L.; Xu, Z.; Huang, L.; Xue, Y.; Geng, D.; Wu, B.; Hu, W.; Yu, G.; Liu, Y. *Adv. Mater.* **2014**, *26*, 1348.

(19) Wei, D.; Lu, Y.; Han, C.; Niu, T.; Chen, W.; Wee, A. T. S. *Angew. Chem., Int. Ed.* **2013**, *52*, 14121.

(20) Hong, X.; Posadas, A.; Zou, K.; Ahn, C. H.; Zhu, J. *Phys. Rev. Lett.* **2009**, *102*, 136808.

(21) Shin, Y.-S.; Son, J. Y.; Jo, M.-H.; Shin, Y.-H.; Jang, H. M. *J. Am. Chem. Soc.* **2011**, *133*, 5623.

(22) Zhang, Y.; Brar, V. W.; Girit, C.; Zettl, A.; Crommie, M. F. *Nat. Phys.* **2009**, *5*, 722.

(23) Xue, J.; Sanchez-Yamagishi, J.; Bulmash, D.; Jacquod, P.; Deshpande, A.; Watanabe, K.; Taniguchi, T.; Jarillo-Herrero, P.; LeRoy, B. J. *Nat. Mater.* **2011**, *10*, 282.

(24) Deak, D. S.; Silly, F.; Porfyrakis, K.; Castell, M. R. *J. Am. Chem. Soc.* **2006**, *128*, 13976.

(25) Reyren, N.; Thiel, S.; Caviglia, A. D.; Kourkoutis, L. F.; Hammerl, G.; Richter, C.; Schneider, C. W.; Kopp, T.; Ruetschi, A. S.; Jaccard, D.; Gabay, M.; Muller, D. A.; Triscone, J. M.; Mannhart, J. *Science* **2007**, *317*, 1196.

(26) Sun, J.; Wu, C.; Silly, F.; Koos, A. A.; Dillon, F.; Grobert, N.; Castell, M. R. *Chem. Commun.* **2013**, *49*, 3748.

(27) Wang, Y.; Ni, Z.; Yu, T.; Shen, Z.; Wang, H.; Wu, Y.; Chen, W.; Wee, A. T. S. *J. Phys. Chem. C* **2008**, *112*, 10637.

(28) Chen, Y.-F.; Bae, M.-H.; Chialvo, C.; Dirks, T.; Bezryadin, A.; Mason, N. *J. Phys.: Condens. Matter* **2010**, *22*, 205301.